Origin of transparency in scattering biomimetic collagen materials

Chrystelle Salameh[a,b,1,2], Flore Salviat[a,b,c,1], Elora Bessot[b], Miléna Lama[b,d], Jean-Marie Chassot[e], Elodie Moulongui[b], Yan Wang[b], Marc Robin[b], Arnaud Bardouil[f], Mohamed Selmane[g], Franck Artzner[f], Alba Marcellan[d], Clément Sanchez[a,b], Marie-Madeleine Giraud-Guille[b], Marco Faustini[b], Rémi Carminati[e], and Nadine Nassif[a,b,e,3]

[a]Collège de France, PSL University, 75231 Paris Cedex 05, France; [b]Sorbonne Université, CNRS, Collège de France, Laboratoire Chimie de la Matière Condensée de Paris (LCMCP), F-75005 Paris, France; [c]Cornea, External Disorders and Refractive Surgery, Fondation Ophtalmologique Rothschild, 75019 Paris, France; [d]Sciences et Ingénierie de la Matière Molle, Ecole Supérieure de Physique et de Chimie Industrielles de la Ville de Paris (ESPCI) Paris, Paris Sciences et Lettres (PSL) University, CNRS, Sorbonne Université, 75005 Paris, France; [e]Institut Langevin, ESPCI Paris, CNRS, PSL University, 75005 Paris, France; [f]CNRS, Institut de Physique de Rennes, UMR 6251, Université de Rennes, F-35000 Rennes, France; and [g]Institut des Matériaux de Paris Centre, Sorbonne Université, 75252 Paris Cedex 05, France

Edited by Lia Addadi, Weizmann Institute of Science, Rehovot, Israel, and approved April 10, 2020 (received for review January 21, 2020)

Living tissues, heterogeneous at the microscale, usually scatter light. Strong scattering is responsible for the whiteness of bones, teeth, and brain and is known to limit severely the performances of biomedical optical imaging. Transparency is also found within collagen-based extracellular tissues such as decalcified ivory, fish scales, or cornea. However, its physical origin is still poorly understood. Here, we unveil the presence of a gap of transparency in scattering fibrillar collagen matrices within a narrow range of concentration in the phase diagram. This precholesteric phase presents a three-dimensional (3D) orientational order biomimetic of that in natural tissues. By quantitatively studying the relation between the 3D fibrillar network and the optical and mechanical properties of the macroscopic matrices, we show that transparency results from structural partial order inhibiting light scattering, while preserving mechanical stability, stiffness, and nonlinearity. The striking similarities between synthetic and natural materials provide insights for better understanding the occurring transparency.

collagen | self-assembly | photonic materials | mechanical properties | transparency

Aside from structural colors and pigmentation, and the usual strong scattering generated by biological tissues, optically transparent or translucent organisms are found in nature. They are quite abundant in aquatic environments (e.g., medusa and planktonic organisms) but rare on land (e.g., the butterfly *Greta oto*). The biological role of transparency appears to be related to protection from predators (1–3). The physical basis of biological transparency is not straightforward. Living tissues are heterogeneous at the submicron and micrometer scales, resulting in spatial fluctuations of the refraction index that are expected to produce light scattering. Deciphering the relation between light scattering and the structure of disordered or partially ordered materials is challenging. However, it is a key step in understanding the appearance of transparency in living organisms, and more generally in natural materials.

Among the few reported transparent biological materials, cornea is a connective tissue that forms the front part of the eye. It works as a refracting lens possessing dioptric properties. Light transmission in healthy corneas occurs through the tissue containing collagen fibrils, proteoglycans, and cells, and scattering from collagen is suppressed by interferences induced by partial order in the fibrillar network. Interestingly, disorders opacifying the cornea are a major cause of refractive errors but also blindness (4). Suppression of scattering is generally a key issue encountered at different levels in the mechanism of vision (5). Hence, particular attention has been paid to the distribution of type I collagen, the principal constituent of the corneal stroma, and the link between the fibrillar network and the unexpected high transmittance (6–9).

Collagen type I, a major structural protein in the body, displays an assembled fibrillar organization in numerous connective tissues such as bone, dermis, and cornea. Depending on the tissue, collagen organizes differently, which leads to specific mechanical properties (from hard to soft) and optical properties (from opaque to transparent) (10). For instance, a cholesteric structure is observed in the compact bone that contributes to its mechanical properties (11), while the tendon is composed of unidirectional collagen fibrils (12). For cornea, collagen fibrils organize in a general lamellar orientation with some local plywood forms (4). Hence, an interesting correlation exists between the collagen phase diagram and the tissue ultrastructure, although the occurrence of collagen liquid-crystal (LC) phases was never demonstrated in vivo (13).

In addition to cornea and fish scales (14), transparent collagen matrices were recently reported in natural tissues, elephant ivory (15) and teeth of the deep-sea dragonfish (16), and in synthetic collagen scaffolds (17). Transparency of such heterogeneous

Significance

Disordered materials with heterogeneities at scales ranging from nano- to micrometers usually scatter visible light and become opaque beyond a certain thickness. However, transparent materials are found in nature. The physical origin of transparency in natural and artificial biopolymer materials is still not fully understood. Here, a gap of transparency is found in synthetic fibrillar collagen matrices within a very narrow range of concentration. The transparency results from structural partial order inhibiting light scattering, while preserving mechanical stability, stiffness, and nonlinearity. The potential to produce biomimetic hydrogels with such striking optical properties by self-assembly opens an interesting route in the study of photonic materials and provides new elements in the understanding of the appearance of transparency in natural materials.

Author contributions: N.N. designed research; C. Salameh, F.S., E.B., M.L., J.-M.C., E.M., Y.W., M.R., A.B., M.S., A.M., M.F., and N.N. performed research; C. Salameh, F.S., E.B., M.L., J.-M.C., F.A., A.M., C. Sanchez, M.-M.G.-G., M.F., R.C., and N.N. analyzed data; and C. Salameh, F.S., M.L., J.-M.C., F.A., A.M., R.C., and N.N. wrote the paper.

The authors declare no competing interest.

This article is a PNAS Direct Submission.

[1]C. Salameh and F.S. contributed equally to this work.

[2]Present address: Institut Européen des Membranes (IEM), UMR 5635, Univ Montpellier, CNRS, Ecole Nationale Supérieure de Chimie de Montpellier (ENSCM), 34095 Montpellier, Cedex 5, France.

[3]To whom correspondence may be addressed. Email: nadine.nassif@sorbonne-universite.fr.

This article contains supporting information online at https://www.pnas.org/lookup/suppl/doi:10.1073/pnas.2001178117/-/DCSupplemental.

First published May 18, 2020.

complex materials remains an intriguing property. It can be present in different degrees, measured by the optical thickness L/ℓ, with L the sample thickness and ℓ the scattering mean free path, the latter being the average distance a photon travels between subsequent scattering events. Understanding whether transparency ($L/\ell << 1$) results from a change in the intrinsic parameter ℓ, correlated to the microstructure, or merely from a small physical thickness L of the observed sample, is crucial. To quantitatively address this issue, it is important to shape the collagen matrices into a design permitting a measurement of ℓ independently of the physical thickness L.

Here, we report on the existence of a transparent domain in the phase diagram of fibrillar collagen, observed in a narrow range of concentration. Below and above this transparency gap, scattering increases substantially. The stability of the matrices over time made it possible to produce three-dimensional (3D) collagen materials up to 1 cm in thickness by different processes. This ensures that a change in transparency is linked to a change in the scattering mean free path ℓ, thus revealing a change in the matrix ultrastructure that depends on the collagen concentration. Around the critical concentration producing the gap in transparency, the material exhibits locally the corneal collagen microstructure, together with optical and mechanical features close to that of real corneas. Before the fibrils' precipitation (fibrillogenesis in vitro), a metastable LC phase with facets ordered into a 3D network forms between the nematic and the precholesteric phases in the lyotropic molecular collagen diagram. The optical microscopy of this phase recalls the DNA precholesteric phase (18) which exhibits a 3D orientational order (19) similar to that observed in transparent decalcified elephant ivory (15). This observation strengthens the hypothesis of the existence of biological LC analogs (20). The resulting 3D fibrillar transparent matrix may be of interest for studying the relationship between the materials structure and the occurring transparency, which remains difficult to assess with natural corneas, for example (21–23), but also for developing keratoprosthesis models. Finally, our understanding of transparency may provide a new approach to the design of photonic materials manufacturable using self-assembly processes.

Collagen Concentration Gradient and Gap in Transparency

Two types of matrices were prepared, characterized by gradient in collagen concentration ranging from ~20 to ~100 mg/mL. For this purpose, two setups were used: 1) the continuous injection/reverse dialysis process (*Methods* and *SI Appendix, Extended Supporting Methods*) described previously for preparing pure or composite materials (24, 25) (Fig. 1*A*) and 2) the evaporation process (26) (*SI Appendix*, Fig. S1) but without homogenization of the acidic collagen solution. A gap of transparency was observed for both matrices after the fibrils' precipitation (Fig. 1*A* and *SI Appendix*, Fig. S1, arrows). Nevertheless, a slight difference in terms of opacity was observed between the two samples. Noticeably, the thicker material (i.e., 1 cm large) synthesized by injection/reverse dialysis was more opaque. The collagen concentration in the transparent domain was determined from quantifying the amount of hydroxyproline by titration. The same concentration was found whatever the process adopted (evaporation or continuous injection/reverse dialysis), which was around 45 mg/mL. Such a gap of transparency found in the fibrillar collagen diagram appears quite counterintuitive since the increase in collagen concentration leads to an increase in fibrillar density and order: the isotropic/anisotropic transition occurring slightly above 40 mg/mL (27). An increase in density and ordering are competing mechanisms that can lead to a suppression of scattering and the appearance of transparency beyond a given concentration threshold. Here, the recovery of opacity at even larger densities, and therefore the nonmonotonic behavior of the scattering mean free path versus concentration, proves the crucial role of the ultrastructure on the optical properties.

This is easily highlighted as follows. A diluted soluble-acidic collagen (2 mg/mL) was concentrated by a slow evaporation (26–28) up to 45 mg/mL. This technique permits an accurate estimation of the concentration during evaporation by simple weighing. The fibrillar collagen matrix in the Petri dish is shown in Fig. 1*B*, red asterisk. A part of the collagen matrix has been removed locally (area 1) to demonstrate the presence of a transparent matrix in the Petri dish. Area 2 shows a fibrillar collagen matrix where a shear stress was applied using a spatula before fibrillogenesis in vitro. This area becomes opaque after the precipitation of the fibrils, indicating a change in the material's properties. The collagen concentration's being above 40 mg/mL, this should be due to the destabilization of the LC geometry. This observation clearly shows that, in addition to the collagen density, the ultrastructure is of primary importance for the occurring transparency.

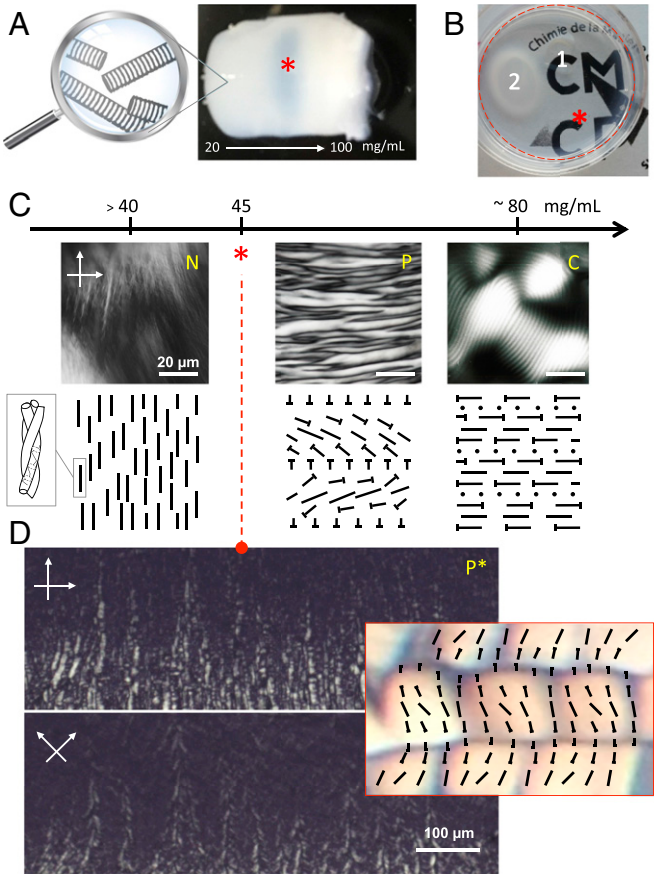

Fig. 1. Optical relationships between collagen fibrillar gradient and LC phase diagram. Images of a fibrillar collagen matrices (*A* and *B*). (*A*) The matrix is characterized by a gradient in concentration (20 to 50 to 100 mg/mL range) and exhibits a gap of transparency. (*B*) The matrix (red asterisk) which is delimited by the red dotted circle is fully transparent in the Petri dish; the final concentration of collagen is ~45 mg/mL. Two other areas are observed: 1 is vacant and 2 is opaque after shearing. (*C*) Classical collagen phase diagram (scheme and polarized optical micrograph) from nematic (N) to cholesteric (C) observed between crossed polarizers (0 to 90°). Segments are molecules in the section plane; dots are molecules normal to this plane; nails are molecules in oblique position with the head representing the molecular extremity pointing toward the observer. The collagen phase diagram is implemented with a new precholesteric phase (P*) for which concentration is found around 45 mg/mL. For the P*, the birefringent texture appears as cubic platelets (*D*). This faceted pattern is still observed after a 45° polarizer rotation; the organization of collagen molecules for P* is presented schematically in the red framed image at higher magnification (*SI Appendix*, Fig. S2 *A* and *B*). The precholesteric phase (P) occurs by increasing the collagen concentration in the solution.

The phase diagram of collagen molecules has been extensively studied (29) (Fig. 1*C*) and exhibits three arrangements: nematic (above 40 mg/mL) (N in Fig. 1*C*), precholesteric (P in Fig. 1*C*), and cholesteric (above ∼75 mg/mL) (27) (C in Fig. 1*C*). None of them was described to lead to transparent collagen materials, although thermotropic nematic liquid crystals tend to be relatively translucent (liquid-crystal displays).

The fact that the physical properties recorded on the transparent matrices remain similar whatever the source of collagen (the porcine clinical grade and the one extracted from rat tails tendons; *SI Appendix*, *Extended Supporting Methods*) ensured that the concentration protocols are 1) reproducible for generating the transparency and 2) that geometry, at a certain collagen concentration, is the key factor for the matrix transparency. Previous work in the literature described the formation of transparent but very thin collagen matrices (30, 31) for which the transparency appears stable at acidic pH (3.5) and is only related to a specific ionic strength, thus rendering comparison with our work difficult.

Further investigations of the collagen phase diagram were done handling the solutions with care. For this purpose, an acidic solution of collagen concentrated at 40 mg/mL was deposited between slide and coverslip and studied by polarized light microscopy, the concentration of collagen occurring at the air/solution interface through a slow evaporation of solvent. The evaporation of solvent being not homogeneous over the drop, the precise concentrations remain uncertain. Acidic collagen solutions with a 2-mm thickness are transparent under ∼100 mg/mL (32). As expected, first a nematic phase is observed where the molecules orient themselves in the same direction (Fig. 1*C*, N). Second, when we slowly evaporate the collagen solution reaching 44 mg/mL, a facetted pattern starts to appear (Fig. 1*D* and *SI Appendix*, Fig. S2) with the presence of stripes in some domains (*SI Appendix*, Fig. S2 *A* and *B*). The facets are polydisperse in size and organize mostly as a mosaic (*SI Appendix*, Fig. S2 *C*–*C*′). Nevertheless, the bigger ones locally arrange in layers reminding the fibrillar collagen arrangement in mice corneal stroma (33) and coelacanth scales (14). The facetted organization of collagen molecules seems different from the "staggered dots" texture described previously in the literature for collagen since it was observed over the cholesteric phase (34) and not related to any optical property. Finally, controlling the sample thickness and the conditions of observations (temperature, humidity, and time under the microscope light) slowed down its systematic transformation into the most common precholesteric phase with a "banded" structure but did not avoid it (*SI Appendix*, Fig. S2*D*). Note that a color phase possessing a filament texture was sometimes observed (35) (*SI Appendix*, Fig. S3*A*), but only with the highly purified clinical-grade collagen (*SI Appendix*, Fig. S3*B*). The transition between the nematic and the precholesteric phases occurs around 46 to 47 mg/mL. The fact that the mosaic phase appears in a very narrow range of concentrations (∼44 to 45 mg/mL) may explain why it was never identified before. Interestingly, after a 45° polarizer rotation, some vertical areas (Fig. 1*D*) remain gray, indicating a vanishing birefringence, while the intensities of areas within these lines are very sensitive to the cross-polarizer orientation. Note that with one polarizer blue and brownish colors were observed, remaining unchanged locally when the stage was rotated (*SI Appendix*, Fig. S2*B*). Such observations indicate a 3D orientational order that has been characterized in blue phases of chiral thermotropic liquid crystals (36) and shortened lyotropic double-stranded DNA solutions (19). The size of the biomacromolecules (DNA and collagen) is noticeably much longer than the thermotropic molecules. Finally, the local arrangements of nonfluid analogs in annelid cuticle (37) and boxfish scutes (38) reports on the analogy between the 3D fibrils' order and a blue phase geometry, although the existence of an LC state is not demonstrated. The polarizing light microscopy images are not in agreement with these previously observed phases. Indeed, all these models exhibit a cubic symmetry and are thus incompatible with the experimental observations of a preferential direction of low birefringence lines. A new model is consequently required. It should exhibit 1) 3D orientational order and 2) large oscillations (>40°) of the orientation of the birefringence director. Such a model is proposed in Fig. 1*D* (scheme) and is in agreement with all optical microscopy observations. This is an intermediate organization between the twisted nematic (39) and the helicoidal instability observed in the cholesteric phase (40). Interestingly, the molecular orientation is continuous at long range, and the 3D orientational order of collagen matrices recalls that of the structure in decalcified elephant ivory (15), although the scale is different. The organization here does not present any defects that are required between the double-twist cylinders in 3D-ordered chiral mesophases, ensuring the high optical transparency of the fibrillar matrix. Indeed, such defects in blue phases exhibit huge refractive index variation and are at the origin of light interferences (color) and scattering (turbidity).

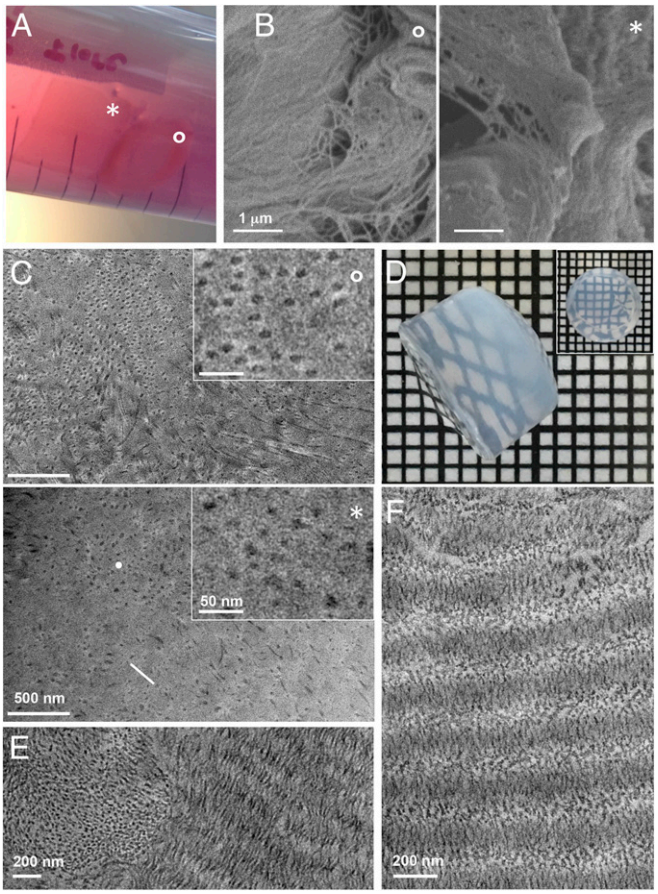

Fig. 2. Ultrastructure investigations of optically transparent collagen-based materials by electron microscopies. (*A*) The collagen matrix (*) and the cornea (°) stored in Cornea Cold as classical storage medium. Both samples remain transparent when stored in the medium. (*B*) SEM and (*C*) TEM images of the biological cornea (°) and the synthetic transparent collagen matrix (*). (Scale bars, 1 μm [*B*] and 500 nm [*C*].) Insets in *C* are observations at higher magnification. (Scale bars, 50 nm.) The fibrils lay parallel (white line) or perpendicular (white dot) to the section cut. (*D*) Thick 3D fibrillar collagen matrix (1 cm in diameter) with a narrow gradient of concentration prepared by using the injection/reverse dialysis process to reach a final concentration around 45 mg/mL over the bulk. An optical gradient of transparency is observed going from opalescent (higher concentration) to transparent (lower concentration) from the curve side but is entirely transparent when observed from the flat end (*Inset*). (*E* and *F*) TEM images of the opalescent collagen matrix showing orthogonal arrangements of the fibrils reminding that of the corneal stroma.

To improve our understanding of the origin of transparency in collagen structures, observations were performed on pig corneas without polarization (*SI Appendix*, Fig. S4*A*). Corneal birefringence is known and varies within a single cornea. Birefringent domains are observed under physical constraints (*SI Appendix*, Fig. S4*B*) which at higher magnification appear as a layered texture (*SI Appendix*, Fig. S4*C*), in agreement with the birefringence texture in mice corneal stroma (33).

In summary, as previously described for transparent collagen matrices of elephant ivory (15), collagen appears to form a precholesteric phase which presents a 3D orientational order. This phase can be interpreted as a subtle equilibrium between double-twist trend for the radial structure of collagen fibrils (41) with only bending deformation, and a helical deformation with a splay deformation. However, due to the lack of crystallographic evidence and physical properties, we will refer to it as precholesteric* phase, P*.

To help identify the physicochemical factors for the origins of the transparency, structural, optical, and mechanical characterization are required.

Ultrastucture of Transparent Collagen Matrices and Analogy with Cornea

Before sample preparation for electron microscopy observations, the synthetic and the biological materials were stored in a classical storage medium for cornea (i.e., Cornea Cold; *SI Appendix*, *Extended Supporting Methods*). Both were stable and remain transparent in the medium (Fig. 2*A*). This step allows a safe comparison of the materials in discarding any potential effect that would have been induced by different ionic forces, pH, and so on on the observed ultrastructure.

Scanning electron microscopy (SEM) observations were performed on a pig cornea (Fig. 2*B*, °) and compared to a transparent collagen matrix (∼45 mg/mL) (Fig. 2*B*, *). Both exhibit dense network with thin collagen fibrils (≤ 100 nm). Transmission electron microscopy (TEM) investigations confirm the high similarity in appearance between the two samples (Fig. 2*C*). Higher magnification (Fig. 2 *C*, *Inset*) shows that fibrils are monodisperse in diameter, which is a main characteristic of biological tissues. The diameter is ∼25 to 30 nm and classical for corneal tissue (42). The extrafibrillar space also appears in the same range of order (≤100 nm) with an average interfibrillar spacing of ∼45 nm in both samples. It is worth mentioning that the formation of biomimetic self-assembled gel needs both an attractive force to gather together the collagen molecules into fibrils and a repulsive force to freeze the fibrils into liquid crystalline order. The balance between the two forces prevents the fibrils from agglomeration, allowing the formation of tissue-like matrices (43). The lack of the other organic constituents (mainly proteoglycans) present in the corneal extracellular matrix may be the reason for the difference in aspects of the collagen. Collagen fibrils appear mostly aligned parallel (line) or perpendicular (dot) to the section plane, recalling previous observations performed with clustered DNA bundles (19), although a periodic pattern is difficult to draw (*SI Appendix*, Fig. S5). This is in fact also the case for cornea when the section plane is not perfectly performed perpendicular (*SI Appendix*, Fig. S6*A*) avoiding the observation of the organized orthogonal plywood (*SI Appendix*, Fig. S6*B*). This is quite intriguing since transparency of cornea is usually related to the arrangement of fibrils in a lattice with a high degree of order (6–8). Although short-range order is certainly a key ingredient for transparency, the microstructure of cornea on a large scale appears to be more complex.

To improve our understanding of the correlation between the microstructure of the collagen material and its transparency, further investigations were performed on a material larger in size (cylinder ∼0.5 × 1 cm^2) with a final concentration of ∼45 mg/mL. Although the material is indeed transparent from the flat end (Fig. 2 *D*, *Inset*), a gradient of transparency forms going from opalescent to completely transparent when observed from the curve side as depicted in Fig. 2*D*. This indicates a slight difference in concentration in the collagen material ($\Delta C \leq 1$). The ultrastructure was investigated by TEM, revealing two other orthogonal arrangements of fibrils in the opalescent domain (Fig. 2 *E* and *F*). Their spatial distribution appears heterogeneous over the domain but we cannot exclude that there is in fact a link between their position and a specific concentration. Both domains are denser in collagen fibrils.

One presents two types of bundles of fibrils (Fig. 2*E*), each showing a constant orientation, but abrupt angular changes at the transition from one bundle to the next one. Interestingly, this arrangement recalls that of fish scutes (*SI Appendix*, Fig. S7*A*) where an analogy with a blue phase geometry is made (14, 38). This original architecture can also be compared to the arrangement found in decalcified ivory of elephant (15, 44). Noticeably, the 3D helical arrangement is observed at higher scale but remains optically transparent (*SI Appendix*, Fig. S7*B*).

The other domain presents two types of layers of fibrils. Each layer shows a constant orientation. As for the two other domains, the collagen fibrils are observed either in cross-section or in longitudinal section being systematically at approximate right angles to the surrounding layers. Thus the synthetic opalescent domain exhibits high similarities in terms of structure (i.e., local orthogonal plywood of lamellae) and size (i.e., fibril diameter, intermolecular packing [*SI Appendix*, Fig. S8], and thickness of layers) (45) with the corneal stroma (*SI Appendix*, Fig. S6*B*). Although the orientation of the collagen fibrils in longitudinal section is perpendicular to the usual but very local observations found in the literature as discussed above, it is also found in cornea (*SI Appendix*, Fig. S6*A*, rectangle).

In summary, three domains exhibit very thin and regular fibril diameter with orthogonal arrangements (from single fibril to layers or bundles of fibrils). The domains coexist in the gap of transparency in the fibrillar collagen diagram. According to this noticeable difference in the domains' size, it may be proposed that the ratio between the unit (whatever its nature, e.g., collagen fibril or empty tubule) and an associate orthogonal arrangement is the key for building transparent materials. To go further on the understanding of the structural–property relationship, the intrinsic degree of transparency (scattering mean free path) was investigated on materials evolving from transparent to opaque and compared to the cornea biological tissue. In addition, mechanical investigations were performed to help identify the physicochemical parameters involved in the formation of such optical properties.

Correlation Between Microstructure and Optical and Mechanical Properties

A set of homogeneous matrices with a thickness of ∼2 mm was prepared using the slow evaporation process described above (*SI Appendix*, *Extended Supporting Methods*), with concentrations ∼40, ∼42, ∼43.5, ∼45, ∼47, and ∼48 mg/mL, covering a narrow range around the critical concentration 45 mg/mL. Transmittance spectra of hydrated fibrillar collagen matrices recorded in the visible and near-ultraviolet, and normalized by the transmittance of the more transparent sample (*SI Appendix*, *Extended Supporting Methods*), are shown in Fig. 3*A*. Increased transmittance of the ∼45 mg/mL matrix is observed over the full wavelength range, which provides qualitative support to the change in transparency. For a quantitative assessment of the degree of transparency, we measured the scattering mean free path ℓ using full-field optical coherence tomography (OCT) (46) (Fig. 3 *B*–*E*). The spatially averaged OCT signal decays exponentially with depth within the material, with a characteristic decay length ℓ, thus providing a direct measurement of this intrinsic parameter in scattering materials (*SI Appendix*, *Extended Supporting Methods*). First, measurements were performed on an ex vivo pig cornea (Fig. 3*B*). A typical in-depth OCT cross-section (Fig. 3*C*) clearly shows the decreasing OCT signal from which the value of ℓ is extracted.

Measurements in four different zones (indicated as square regions in Fig. 3*B*) are presented in a bar graph, showing an increased transparency in the center, consistent with the visual appearance of the cornea. Second, investigations were conducted on the matrix made with the broad gradient in collagen concentration as shown in Fig. 1*A* (Fig. 3 *D* and *E*). The scattering mean free path ℓ was measured in seven different zones, with decreasing concentration in collagen, resulting in the bar graph in Fig. 3*D*. Substantial changes, by almost a factor of 2, are observed along the collagen concentration gradient, and thus by moving through different fibrillar microstructures. Larger values of ℓ at the center indicate an increase in transparency, in agreement with visual appearance and the transmittance curves. This substantial change in ℓ is a signature of the crucial role of partial short-range order in disordered scattering materials. Indeed, it is known that variations of partial order in the fibrils positions can lead to smaller or larger values of ℓ (47, 48), up to transparency (49). Interestingly, the value $\ell = 125.4$ μm found in the center of the pig cornea (Fig. 3*B*) is on the order of the values ℓ ∼120 to 140 μm measured at the edges of the transparency gap of the gradient matrix (zones 1 and 4 in Fig. 3*D*). This correspondence is supported qualitatively by the in-depth OCT cross-section images (Fig. 3*E*) of the 3D synthetic bulk (∼45 mg/mL; Fig. 2*D*). Indeed, we observe that the collagen fibrils are parallel and superimposed in the opalescent part (corresponding to the edge of the transparency gap), recalling the structure of the corneal stroma (Fig. 3*C*). This strengthens the hypothesis that increased partial order at a concentration 45 ± 1 mg/mL is responsible for enhanced transparency. This also suggests that the structure of cornea may not correspond to the maximum of transparency, presumably since other properties (e.g., mechanical) also need to be optimized.

Based on the evidence of the crucial role of the ultrastructure on the optical properties, the mechanical properties of the collagen matrices were also investigated. The transparent matrix at ∼45 mg/mL is tough and easy to handle (Movie S1). It remains transparent upon mechanical handling and shearing, suggesting that fibrillar rearrangements do not operate at the scale of visible wavelengths (from ∼100 nm to a few micrometers). However, gel stability is very sensitive to slight differences in concentration (*SI Appendix*, Fig. S9). This suggests that the assumed improvement of mechanical properties of collagen fibrillar matrices with concentration described in the literature (30, 50) does not necessarily apply around the concentration leading to transparency.

More quantitative assessment of the mechanical response of optically transparent materials with concentrations in the range ∼43 to 45 mg/mL was obtained at large strains in tension and compared to freshly extracted cornea. The general mechanical response of the matrices exhibits biomimetic mechanical behavior. Tensile behavior of the fibrillar matrices is strongly nonlinear (Fig. 4), with extreme compliance at the lower stretches and hardening at intermediate strains, as expected for biological tissues (51–53) and more especially for cornea (54). From this "J-shaped" mechanical response, elastic moduli were defined in the toe and linear region, respectively.

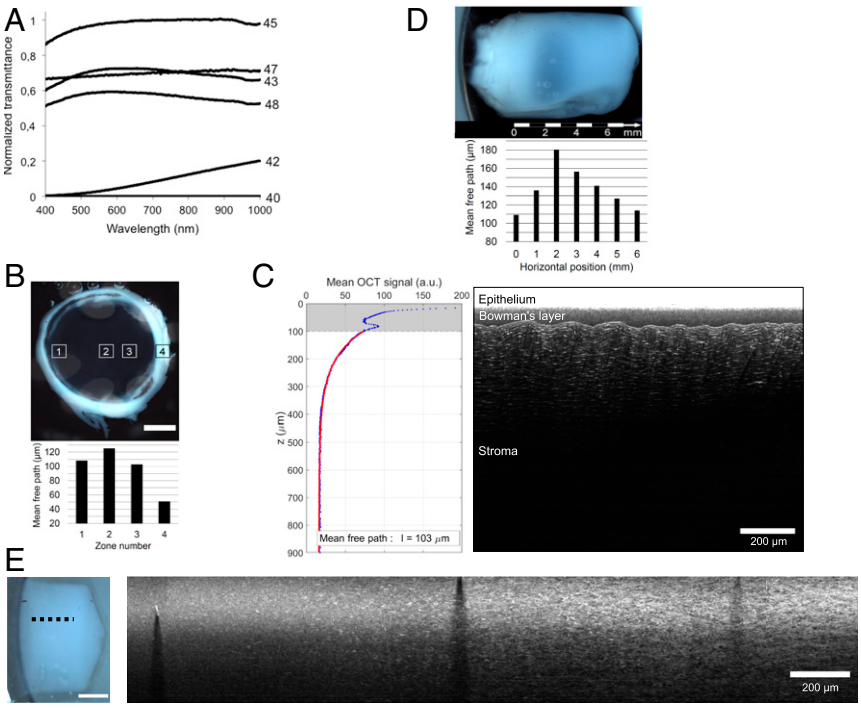

Fig. 3. Transparency of a freshly extracted pig cornea and of collagen matrices investigated by transmittance (*A*) and full-field OCT (*B*–*E*). (*A*) Transmittance spectra of collagen matrices for visible and near-infrared wavelengths are provided for concentrations ranging from 40 to 48 mg/mL. (*B*) Pig cornea over the black background of the sample holder (*Top*), and bar graph of the measured values of the scattering mean free path ℓ (*Bottom*) in four 1.3- × 1.3-mm^2 zones in the stroma (zones 1 through 3) and in the sclera (zone 4). Larger values of ℓ correspond to an increase in transparency. (*C*) In-depth OCT cross-section image in zone 3 (*Right*) from which ℓ is extracted by fitting the average OCT signal versus the depth z (*Left*, blue dots) with an exponential decay exp(−z/ℓ) (*Left*, red curve; values in the gray zone are discarded in the fitting procedure). (*D*) Collagen matrix (characterized by a gradient in concentration [20 to 50 to 100 mg/mL range; see Fig 1*A*]) over the black background of the sample holder (*Top*), and measured values of ℓ (*Bottom*) in seven 100- × 100-μm^2 zones, evenly spaced along a horizontal line, parallel to the collagen concentration gradient in the matrix. The general shape of the bar graph and the maximum value of ℓ measured in the third zone are consistent with the visual observation of maximum transparency in the center of the matrix. (*E*) Collagen matrix (with a narrow gradient of concentration around 45 mg/mL over the 1-cm bulk; see Fig. 2*D*) over the white background of the sample holder (*Left*), and in-depth OCT cross-section image (*Right*) along the collagen concentration gradient (black dashed line in *E*, *Right*). The change in the structural appearance of the matrix is clearly visible (from left to right in the OCT cross-section), with an increasing textured aspect.

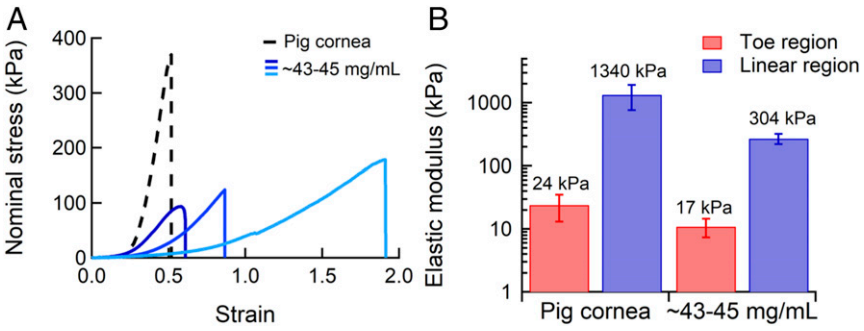

Fig. 4. Mechanical behavior (tension mode) of transparent collagen matrices and of freshly extracted pig cornea. (*A*) The three fibrillar collagen gels prepared by injection/reverse dialysis approach at concentrations in the range ~43 to ~45 mg/mL exhibit a "J-shaped" stress–strain response, as observed for biological tissues. As a guideline, the mechanical response of the pig cornea is given. No preconditioning was applied, that is, curves correspond to the first loading. Note that the maximal stress value before rupture, usually defined as the ultimate tensile strength (UTS), is only indicative since gel (as cornea) failure systematically occurred in the clamps, suggesting that clamps involve local premature damage. (*B*) Modulus increasing with extension, elastic moduli are given in the toe and linear region, respectively. Gel rigidities display moduli of same order of magnitude.

Performing such large strain characterizations on hydrated materials is delicate due to their intrinsic softness and wetness that necessitate preventing any slippage in the jaws and drying during the tests (55). Besides, their potential drying can induce a collapse of the fibrillar collagen network, dramatically enhancing the stiffness (56). The elastic moduli in the linear region of the transparent collagen matrices in the range ~43 to 45 mg/mL (304 ± 50 kPa) are consistent with the higher values found in the literature after the critical concentration threshold for anisotropic fibrillar arrangement (50, 57). However, the stiffness of the transparent matrices in the linear regime is about fourfold lower than that of the pig cornea (1,340 ± 580 kPa) (30). These differences can be explained by the presence of components in the cornea that play an important role in ensuring the mechanical performance (56). The presence of a "nonfibrillar organic matrix" (including proteoglycan), which resists the separation of the fibrils during shearing, was reported in bone tissue (58) and may exist for the synthetic collagen matrix made of residual components not extracted from the purification step (*SI Appendix*, Fig. S3*B*) and/or collagen molecules that did not precipitate. Furthermore, our process does not enable a precise spatial control of the anisotropy in 3D at the microscale, which increases the variability of the mechanical behavior even in a narrow concentration range. Note that ultimate stages of the stress-strain curves were truncated when macroscopic damage (crack) appeared in the sample. Ultimate tensile stresses and strains at break were not investigated, as failure systematically occurred in the clamps. It is worth mentioning that a pretreatment of collagen-based materials is quite systematically used in the literature to reinforce their mechanical properties by means of reticulant agents (59, 60).

In conclusion, we have demonstrated the existence of a gap of transparency in synthetic collagen matrices, around a critical collagen concentration of 45 mg/mL. Transparency is observed for a narrow range of concentrations, below a few milligrams per milliliter, that corresponds to a specific precholesteric phase in the molecular collagen diagram. This phase presents a 3D orientational order without collagen director linear singularity such as disclination. The intimate connection between the degree of optical transparency and the microstructure has been addressed quantitatively. Transparency emerges from structural correlations in the fibrillar collagen network that inhibit light scattering and coexists with a biomimetic mechanical response. The possibility to produce hydrogels by biopolymer self-assembly with such striking optical properties opens a very interesting route in the study of photonic materials. The synthetic collagen matrix also bears deep resemblance to natural corneal stroma, in terms of microstructure and macroscopic optical and mechanical properties. This strengthens the hypothesis of the existence of biological LC analogs to form 3D tissue architectures with specific emerging properties.

Methods

Full details of sample preparation and characterization techniques (polarized light microscopy, SEM, TEM, small-angle X-ray scattering, transmittance, full-field OCT, and tensile testing) are presented in *SI Appendix, Extended Supporting Methods*. This includes the collagen and cornea sources, the collagen gradient matrices synthesis (evaporation procedure and injection/reverse dialysis), and the collagen matrices storage and stability. Briefly, two sources of type I collagen were used either extracted from rat tail tendons or purchased from Symatèse. The synthesis of collagen gradient matrices was performed by either slow evaporation under a laminar flow hood or by injection/reverse dialysis.

Data Availability. The data supporting the findings of this study are available within the paper and *SI Appendix*.

ACKNOWLEDGMENTS. N.N. thanks the Fondation Collège de France and Fondation Electricité de France for financial support, especially Marie Cheron for sharing opinions and her trust, Jean-Baptiste Hennequin (Ecole Supérieure de Physique et Chimie Industrielles de Paris [ESPCI Paris]) for the spark that led to the collaboration of the coauthors, and Niki Baccile (Laboratoire Chimie de la Matière Condensée de Paris [LCMCP]) for fruitful discussion about small-angle X-ray scattering data. We thank Josette Legagneux (Institut de Chirurgie, Paris) for providing pig cornea; Christophe Helary (LCMCP) for help with electrophoresis; and Bernard Haye (LCMCP) for preparation of some TEM samples.

1. W. C. Kerfoot, A question of taste: Crypsis and warning coloration in freshwater zooplankton communities. *Ecology* **63**, 538–554 (1982).
2. J. R. M. Langsdale, Developmental changes in the opacity of larval herring, Clupea harengus, and their implications for vulnerability to predation. *J. Mar. Biol. Assoc. U. K.* **73**, 225–232 (1993).
3. A. Tsuda, S. Hiroaki, T. Hirose, Effect of gut content on the vulnerability of copepods to visual predation. *Limnol. Oceanogr.* **43**, 1944–1947 (1998).
4. K. M. Meek, C. Knupp, Corneal structure and transparency. *Prog. Retin. Eye Res.* **49**, 1–16 (2015).
5. M. Kreysing, L. Boyde, J. Guck, K. J. Chalut, Physical insight into light scattering by photoreceptor cell nuclei. *Opt. Lett.* **35**, 2639–2641 (2010).
6. D. M. Maurice, The structure and transparency of the cornea. *J. Physiol.* **136**, 263–286 (1957).
7. R. W. Hart, R. A. Farrell, Light scattering in the cornea. *J. Opt. Soc. Am.* **59**, 766–774 (1969).
8. G. B. Benedek, Theory of transparency of the eye. *Appl. Opt.* **10**, 459–473 (1971).
9. T. J. Freegard, The physical basis of transparency of the normal cornea. *Eye (Lond.)* **11**, 465–471 (1997).
10. D. J. Prockop, What holds us together? Why do some of us fall apart? What can we do about it? *Matrix Biol.* **16**, 519–528 (1998).
11. M.-M. Giraud-guille, Cholesteric twist of collagen in vivo and in vitro. *Mol. Cryst. Liq. Cryst. Incorp. Nonlin. Optics* **153**, 15–30 (1987).

12. S. Weiner, W. Traub, H. D. Wagner, Lamellar bone: Structure-function relations. *J. Struct. Biol.* **126**, 241–255 (1999).
13. M. Mitov, Cholesteric liquid crystals in living matter. *Soft Matter* **13**, 4176–4209 (2017).
14. M. M. Giraud, J. Castanet, F. J. Meunier, Y. Bouligand, The fibrous structure of coelacanth scales: A twisted "plywood". *Tissue Cell* **10**, 671–686 (1978).
15. M. Albéric, A. Gourrier, W. Wagermaier, P. Fratzl, I. Reiche, The three-dimensional arrangement of the mineralized collagen fibers in elephant ivory and its relation to mechanical and optical properties. *Acta Biomater.* **72**, 342–351 (2018).
16. A. Velasco-Hogan *et al*., On the nature of the transparent teeth of the deep-sea dragonfish, Aristostomias scintillans. *Matter* **1**, 235–249 (2019).
17. A. Tidu *et al*., Highly concentrated collagen solutions leading to transparent scaffolds of controlled three-dimensional organizations for corneal epithelial cell colonization. *Biomater. Sci.* **6**, 1492–1502 (2018).
18. F. Livolant, Precholesteric liquid crystalline states of DNA. *J. Phys. France* **48**, 1051–1066 (1987).
19. A. Leforstier, F. Livolant, DNA liquid crystalline blue phases. Electron microscopy evidence and biological implications. *Liq. Cryst.* **17**, 651–658 (1994).
20. Y. Bouligand, Twisted fibrous arrangements in biological materials and cholesteric mesophases. *Tissue Cell* **4**, 189–217 (1972).
21. K. M. Meek, Corneal collagen-its role in maintaining corneal shape and transparency. *Biophys. Rev.* **1**, 83–93 (2009).
22. R. L. Trelstad, A. J. Coulombre, Morphogenesis of the collagenous stroma in the chick cornea. *J. Cell Biol.* **50**, 840–858 (1971).
23. V. M. Borderie *et al*., Banding patterns: Exploring a new feature in corneal stroma organization. *ARVO Annu. Meet.* **58**, 3906 (2017).
24. Y. Wang *et al*., Controlled collagen assembly to build dense tissue-like materials for tissue engineering. *Soft Matter* **7**, 9659–9664 (2011).
25. Y. Wang *et al*., The predominant role of collagen in the nucleation, growth, structure and orientation of bone apatite. *Nat. Mater.* **11**, 724–733 (2012).
26. L. Bessea, B. Coulomb, C. Lebreton-Decoster, M.-M. Giraud-Guille, Production of ordered collagen matrices for three-dimensional cell culture. *Biomaterials* **23**, 27–36 (2002).
27. M.-M. Giraud-Guille, Liquid crystallinity in condensed type I collagen solutions. A clue to the packing of collagen in extracellular matrices. *J. Mol. Biol.* **224**, 861–873 (1992).
28. C. Helary, A. Foucault-Bertaud, G. Godeau, B. Coulomb, M. M. G. Guille, Fibroblast populated dense collagen matrices: Cell migration, cell density and metalloproteinases expression. *Biomaterials* **26**, 1533–1543 (2005).
29. F. Gobeaux *et al*., Cooperative ordering of collagen triple helices in the dense state. *Langmuir* **23**, 6411–6417 (2007).
30. A. Tidu *et al*., Development of human corneal epithelium on organized fibrillated transparent collagen matrices synthesized at high concentration. *Acta Biomater.* **22**, 50–58 (2015).
31. P. D. S. Peixoto *et al*., Achievement of cornea-like organizations in dense collagen I solutions: Clues to the physico-chemistry of cornea morphogenesis. *Soft Matter* **9**, 11241–11248 (2013).
32. F. Gobeaux *et al*., Fibrillogenesis in dense collagen solutions: A physicochemical study. *J. Mol. Biol.* **376**, 1509–1522 (2008).
33. M. Aldrovani, A. M. A. Guaraldo, B. C. Vidal, Optical anisotropies in corneal stroma collagen fibers from diabetic spontaneous mice. *Vision Res.* **47**, 3229–3237 (2007).
34. P. D. S. Peixoto, A. Deniset-Besseau, M.-C. Schanne-Klein, G. Mosser, Quantitative assessment of collagen I liquid crystal organizations: Role of ionic force and acidic solvent, and evidence of new phases. *Soft Matter* **7**, 11203–11210 (2011).
35. I. Dierking, Chiral liquid crystals: Structures, phases, effects. *Symmetry* **6**, 444–472 (2014).
36. C. Bahr, H.-S. Kitzerow, *Chirality in Liquid Crystals*, (Springer, 2001).
37. L. Lepescheux, Spatial organization of collagen in annelid cuticle: Order and defects. *Biol. Cell* **62**, 17–31 (1988).
38. L. Besseau, Y. Bouligand, The twisted collagen network of the box-fish scutes. *Tissue Cell* **30**, 251–260 (1998).
39. V. Borshch *et al*., Nematic twist-bend phase with nanoscale modulation of molecular orientation. *Nat. Commun.* **4**, 2635 (2013).
40. F. Lequeux, M. Kléman, Helicoidal instability in cholesteric capillary tubes. *J. Phys. France* **49**, 845–855 (1988).
41. A. I. Brown, L. Kreplak, A. D. Rutenberg, An equilibrium double-twist model for the radial structure of collagen fibrils. *Soft Matter* **10**, 8500–8511 (2014).
42. Y. Komai, T. Ushiki, The three-dimensional organization of collagen fibrils in the human cornea and sclera. *Invest. Ophthalmol. Vis. Sci.* **32**, 2244–2258 (1991).
43. M. M. Giraud-Guille, G. Mosser, E. Belamie, Liquid crystallinity in collagen systems in vitro and in vivo. *Curr. Opin. Colloid Interface Sci.* **13**, 303–313 (2008).
44. M. Albéric *et al*., Relation between the macroscopic pattern of elephant ivory and its three-dimensional micro-tubular network. *PLoS One* **12**, e0166671 (2017).
45. T. Sibillano *et al*., Interfibrillar packing of bovine cornea by table-top and synchrotron scanning SAXS microscopy. *J. Appl. Cryst.* **49**, 1231–1239 (2016).
46. L. Vabre, A. Dubois, A. C. Boccara, Thermal-light full-field optical coherence tomography. *Opt. Lett.* **27**, 530–532 (2002).
47. L. F. Rojas-Ochoa, J. M. Mendez-Alcaraz, J. J. Sáenz, P. Schurtenberger, F. Scheffold, Photonic properties of strongly correlated colloidal liquids. *Phys. Rev. Lett.* **93**, 73903 (2004).
48. K. Vynck, M. Burresi, F. Riboli, D. S. Wiersma, Photon management in two-dimensional disordered media. *Nat. Mater.* **11**, 1017–1022 (2012).
49. O. Leseur, R. Pierrat, R. Carminati, High-density hyperuniform materials can be transparent. *Optica* **3**, 763–767 (2016).
50. S. Ramtani, Y. Takahashi-Iniguez, C. Helary, D. Geiger, M. M. G. Guille, Mechanical behavior under unconfined compression loadings of dense fibrillar collagen matrices mimetic of living tissues. *J. Mech. Med. Biol.* **10**, 35–55 (2010).
51. Y. C. Fung, Elasticity of soft tissues in simple elongation. *Am. J. Physiol.* **213**, 1532–1544 (1967).
52. J. D. Humphrey, Continuum biomechanics of soft biological tissues. *Proc. R. Soc. London. Ser. A* **459**, 3–46 (2003).
53. S. Rose *et al*., Nanoparticle solutions as adhesives for gels and biological tissues. *Nature* **505**, 382–385 (2014).
54. S. Kling, F. Hafezi, Corneal biomechanicsA review. *Ophthalmic Physiol. Opt.* **37**, 240–252 (2017).
55. S. Rose, A. Dizeux, T. Narita, D. Hourdet, A. Marcellan, Time dependence of dissipative and recovery processes in nanohybrid hydrogels. *Macromolecules* **46**, 4095–4104 (2013).
56. D. A. Hoeltzel, P. Altman, K. Buzard, K. Choe, Strip extensiometry for comparison of the mechanical response of bovine, rabbit, and human corneas. *J. Biomech. Eng.* **114**, 202–215 (1992).
57. N. Nassif *et al*., Self-assembled collagen– apatite matrix with bone-like hierarchy. *Chem. Mater.* **22**, 3307–3309 (2010).
58. G. E. Fantner *et al*., Sacrificial bonds and hidden length dissipate energy as mineralized fibrils separate during bone fracture. *Nat. Mater.* **4**, 612–616 (2005).
59. E. Khor, Methods for the treatment of collagenous tissues for bioprostheses. *Biomaterials* **18**, 95–105 (1997).
60. M. E. Nimni, Glutaraldehyde fixation revisited. *J. Long Term Eff. Med. Implants* **11**, 151–161 (2001).